

PAPER • OPEN ACCESS

Stable thermal transport in reduced graphene-oxide aerogel at elevated temperatures

To cite this article: Prakash C Mahakul *et al* 2020 *Mater. Res. Express* 7 105603


View the [article online](#) for updates and enhancements.



The Electrochemical Society
Advancing solid state & electrochemical science & technology
2021 Virtual Education

Fundamentals of Electrochemistry:
Basic Theory and Kinetic Methods
Instructed by: **Dr. James Noël**
Sun, Sept 19 & Mon, Sept 20 at 12h–15h ET

Register early and save!





PAPER

Stable thermal transport in reduced graphene-oxide aerogel at elevated temperatures

OPEN ACCESS

RECEIVED

17 August 2020

REVISED

23 September 2020

ACCEPTED FOR PUBLICATION

1 October 2020

PUBLISHED

14 October 2020

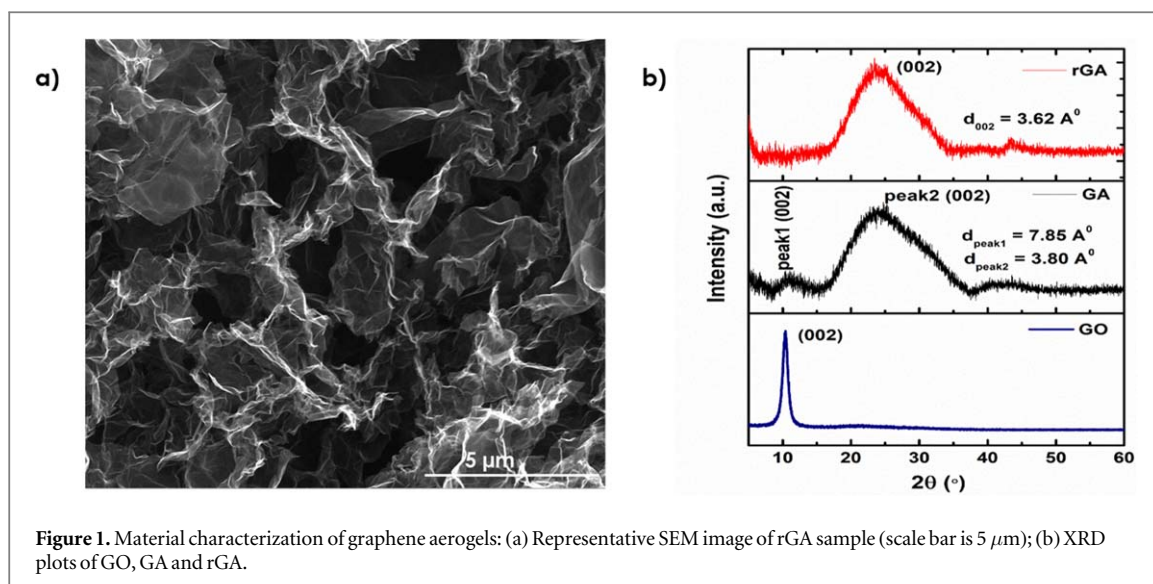
Original content from this work may be used under the terms of the [Creative Commons Attribution 4.0 licence](#).

Any further distribution of this work must maintain attribution to the author(s) and the title of the work, journal citation and DOI.

Prakash C Mahakul^{1,3}, P Gayathri^{1,3}, T Remyamol², H Sreemoolanadhan², M R Ajith² and Manu Jaiswal¹ ¹ Graphene and 2D Systems Laboratory, Department of Physics, Indian Institute of Technology Madras, Chennai 600036, India² Advanced Materials and Ceramics Division, Materials and Metallurgy Group, Vikram Sarabhai Space Centre, Thiruvananthapuram, Kerala, India³ These authors have contributed equally to the work.E-mail: manu.jaiswal@iitm.ac.in**Keywords:** 3D graphene networks, graphene aerogels, thermal insulation, thermal transport, temperature-dependent thermal conductivitySupplementary material for this article is available [online](#)**Abstract**

We investigate thermal transport in three-dimensional graphene aerogel networks at elevated temperatures. The aerogels are solution-processed from graphene-oxide flakes using amine-based linkers and then partially reduced to impart stability in the chemical structure at elevated temperatures. Thermal conductivity of the system is estimated using steady-state electrothermal technique in vacuum in the temperature interval from 30 to 200 °C. The thermal conductivity value is $\kappa \sim 0.2$ W/mK at room temperature, and is found to be weakly dependent on temperature across the entire temperature interval. To examine the microscopic origin of this stable response, the thermal conductivity estimates are complemented with insights from temperature-dependent transient electrothermal response. We show that the temperature stable thermal insulation behaviour observed in this system can be attributed to two factors: point-defect scattering at the flake level from the remnant oxygen-functionalities which dominates over Umklapp scattering processes, and another contribution that arises from interfacial thermal resistance between flakes. The partial reduction thus achieves a delicate balance between imparting chemical stability while also retaining the dominance of point-defect phonon scattering, where the latter contributes to temperature stable thermal conductivity.

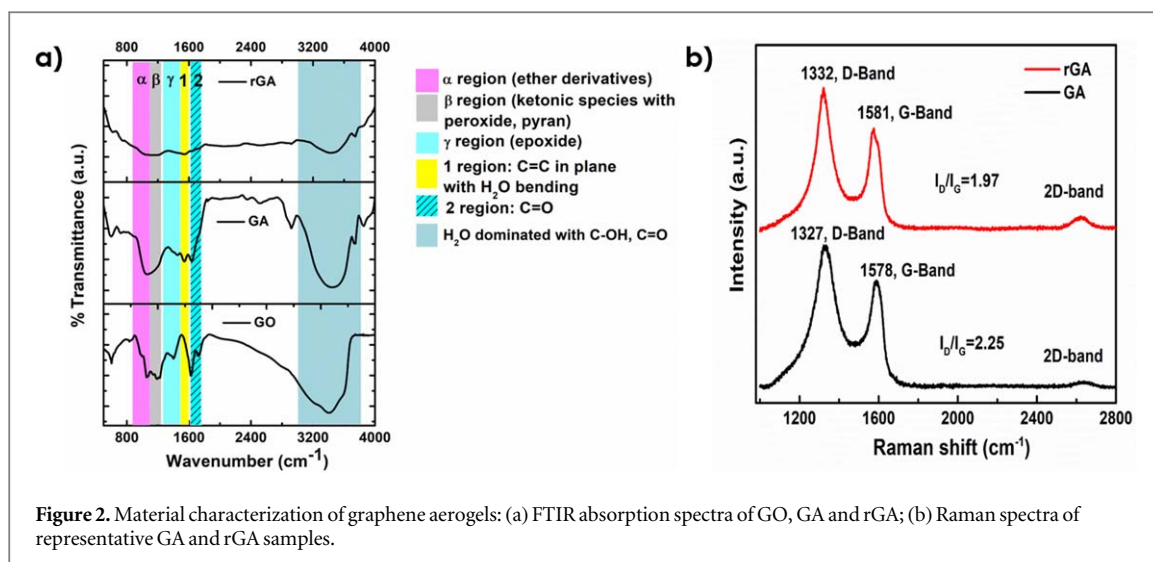
Two-dimensional layered materials can form ultralight porous three-dimensional aerogels. These are candidates for variety of potential applications that include supercapacitors [1], batteries [2], organic solvent absorbers [3], and electromagnetic wave absorbers [4]. Thermal insulation applications of these aerogels have also garnered a lot of interest [5–7]. Till now conventional silica aerogels are popularly used for high temperature thermal insulation applications. Though they possess a small thermal conductivity (κ) of ~ 0.02 W/mK at ambient conditions, they are mechanically very unstable [8]. In contrast, 3D graphene aerogel (GA) constituted from graphene-oxide (GO) flakes possesses very low density and very low thermal conductivity reaching $\kappa \sim 4.6 \times 10^{-3}$ W/mK in ambient condition [6]. Pore-size and defect density are important parameters that govern the thermal conductivity in these systems [9, 10]. While these 3D networks have comparatively better mechanical properties than silica aerogels, they lack thermal stability. In the absence of defects, pristine graphene itself is highly stable up to very high temperatures [11]. The density and nature of oxygen functional groups in GO flakes evolves with annealing [12], as revealed using infra-red spectroscopy techniques [13] or with direct imaging [14]. The confined water trapped in GO flakes, which is gradually expelled with annealing [15], also participates in the chemical processes such as carbonyl formation during annealing [13]. The hydroxyl (–OH) functionalities populating the basal plane are the first to be expelled starting at 75 °C followed by the expulsion of epoxides, carboxyls and ketones at successively higher temperatures of 125 °C, 150 °C and 175 °C respectively. For 200 °C annealing, the hydroxyl and epoxide expulsion was shown to be complete, whereas the decomposition of carboxyls and ketones continued even up to 650 °C annealing, while edge ethers are stable up



to 850 °C. The expulsion of groups also depends on their position in the lattice and for example, at lower temperatures ($T < 200$ °C), the trapped water initiates formation of oxygen containing free radicals which preferentially attack edge functional groups rather than those in the basal plane [13]. Complementing insights have been revealed from XPS spectra, where there is conversion of C=O to C–O groups [16] as well as corresponding enhancements in electrical conductivity owing to increase in size of sp^2 -hybridized graphene islands [17]. Furthermore, the expulsion of oxygen functionalities happens at relatively lower temperatures for the few-layer thick graphene-oxide flakes as compared to thicker flakes. It follows that graphene-oxide aerogels, which are composed of interconnected few-layer graphene-oxide flakes, possess a highly temperature-dependent chemical structure. Annealing therefore causes the physical properties of the aerogels to change continuously with temperature. In this work, we examine the thermal transport in partially reduced graphene-oxide aerogels using electrothermal techniques. The partially reduced material is found to be chemically stable up to the annealing temperature. Interestingly, the thermal conductivity of the aerogel is found to be weakly dependent on temperature in this elevated temperature interval. The steady-state and transient electrothermal data are examined to understand the physical origin of this weak temperature dependence.

Here, 3D graphene aerogels (rGA) have been prepared from graphene-oxide (GO) dispersion (Graphene Laboratories Inc., 4 mg ml^{-1}) using ethylene diamine (EDA) (Sigma Aldrich Co., USA) as a cross-linker by sol-gel routes followed by super critical drying (CPD, Quorum Technologies) as reported earlier [18]. EDA served as the binder for cross-linking the GO sheets to form an interconnected 3D structure. In brief, the required amount of EDA + DI water homogenous mixture was dispersed in the GO solution by mechanical sonication (10 min) followed by continuous stirring for 45 min. Then the GO:EDA dispersion was transferred to a cylindrical vial and baked at 95 °C for 8 h to form the interconnected hydrogel. After cooling down, water from the black and spongy hydrogel was decanted and replaced by solvent exchange process using ethanol as intermediate solvent. For complete water replacement the solvent exchange process was continued for 4–5 days with repeated ethanol replacement in 12 h of interval. Graphene-oxide aerogel (GA) was recovered from the ethanol dispersion without distorting its geometry by supercritical drying using a critical point dryer using liquid CO_2 as the working agent under high pressure [18]. Mechanically-stable samples could be realized with different GO/EDA ratio (v/v) ranging from 0.6×10^3 to 1.1×10^3 with similar material characteristics across the range. Finally, the GA samples were annealed at 200 °C to obtain the reduced graphene-oxide aerogels (rGA). The annealing consisted of ramp up from room temperature to 200 °C in 30 min followed by holding the temperature for 2 h and a slow cool down to room temperature.

We first examine the chemical and physical structure, as well as the microstructure of the samples. From the scanning electron micrographs (Model: INSPECT F50) of a representative rGA sample (figure 1(a)) it can be inferred that the stacks of individual 2D sheets or flakes are well connected to form a 3D porous network. The Brunauer-Emmett-Teller (BET) (Micromeritics ASAP 2020) surface area for GA, prior to annealing, was measured to be $219.2 \text{ m}^2 \text{ g}^{-1}$ with adsorption average pore width of 19.2 nm, while the Barrete-Joynere-Halenda (BJH) adsorption average pore diameter was estimated to be 28.7 nm. Since the porous skeleton morphology is largely preserved during the annealing cycle, the estimates for surface area of rGA will be comparable. These values are similar to those reported in literature, where BET surface area of 130 to $440 \text{ m}^2 \text{ g}^{-1}$ have been reported for graphene oxide and reduced graphene oxide aerogels [9, 19, 20]. The XRD plots of representative GO, GA



and rGA samples are shown in figure 1(b). In both kinds of aerogel samples, a prominent broad peak around 26° is revealed corresponding to an average d-spacing of 0.37 nm between adjacent flakes of a single stack. This suggests partial recovery of the planar sp²-hybridized honeycomb structure when GO is transformed to GA, since the d-spacings in the parent GO solution were about 9 – 10 Å [21]. In addition, the small peak around 10° in GA indicates the presence of some oxidised domains in the sample [22]. Fourier transform infrared (Model: Agilent Cary 600) spectra (see figure 2(a)) of GO contains signatures of oxygen-rich groups, in addition to C=C bonds [23]. Following Acik *et al* [13], the spectral regions can be classified into α (900 – 1100 cm⁻¹), β (1100 – 1280 cm⁻¹), γ (1280 – 1500 cm⁻¹) regions as indicated with the colored bands and these are dominated by modes arising from ether derivatives, ketones and epoxides, respectively with large spectral overlap leading to broadening. Furthermore, the next two band regions are associated with asymmetric vibrational stretching of C=C along with H₂O bending modes (1500 – 1600 cm⁻¹), ketonic and carboxylic groups (1600 – 1750 cm⁻¹). In comparison to GO, the suppression of these oxygen-rich functionalities in GA can be ascribed to an EDA assisted reduction process. The suppression of the broad peak around ~ 3500 cm⁻¹ in rGA shows that the partial reduction process limits the ability of the system to hold intercalated water under ambient conditions, when compared to the as-prepared GO films [23, 24]. In rGA most of the functionalities are further suppressed which suggests annealing assisted further reduction in functional groups. There is further expulsion of the interfacial or confined water interleaved between the flakes. The Raman spectra of representative GA and rGA samples (with GO: EDA ratio of 0.7 × 10³ v/v) are presented in figure 2(b) which shows two prominent bands centred around 1330 cm⁻¹ and 1580 cm⁻¹ corresponding to the D-band and G-band of graphitic structures [25]. The D-band arises from the structural disorder and sp³-hybridized carbon atoms in the graphitic structures whereas the G-band arises from in-plane vibrations of the carbon atoms. The D band to G band intensity ratio for rGA sample is lower (~1.97) compared to that for as-prepared GA sample (~ 2.25), which suggests recovery of the supplemental π – π stacks after thermal annealing [25]. The I_D/I_G ratio in disordered graphene or graphitic systems generally follows a non-monotonic trend. The I_D/I_G ratio initially increases with defect formation when going from graphitic to nanocrystalline forms, and reaches a maximum. Subsequently, the transition from nanocrystalline to amorphous form is associated with decrease in I_D/I_G with increasing defect density [25]. The Raman spectra of the GA and rGA samples indicate that both samples are in the nanocrystalline form, which is consistent with the observations from XRD and FTIR. The temperature dependent properties of rGA are presented in figure 3 and compared with those for GA. The XRD and Raman characterization suggest partial recovery of the planar sp²-hybridized honeycomb structure when GO is transformed to GA and further recovery of the supplemental π – π stacks after thermal annealing. Figure 3(a) shows the thermogravimetric (TGA) (Model: SDT Q600) curve of the as-prepared GA and rGA samples. Between 30 °C and 200 °C, there is a slight weight loss of less than 10% seen in TGA which forms a plateau at the higher temperature. The initial weight loss (<50 °C) can be assigned to the loss of adsorbed gas molecules, especially since the aerogels present very large surface area for a given volume. The response at temperatures above this can be attributed primarily to the expulsion of confined water interleaved between the graphene-oxide sheets, as also revealed from FTIR spectra. The gradual expulsion of functional groups is responsible for the accelerated weight loss above 200 °C. The weight loss in the temperature range 120 °C–180 °C can be ascribed to the evaporation of the intercalated water molecules along with some contribution from loss of oxygen functional groups in GA [26]. In the annealed sample (rGA), the rapid weight loss after 270 °C can be

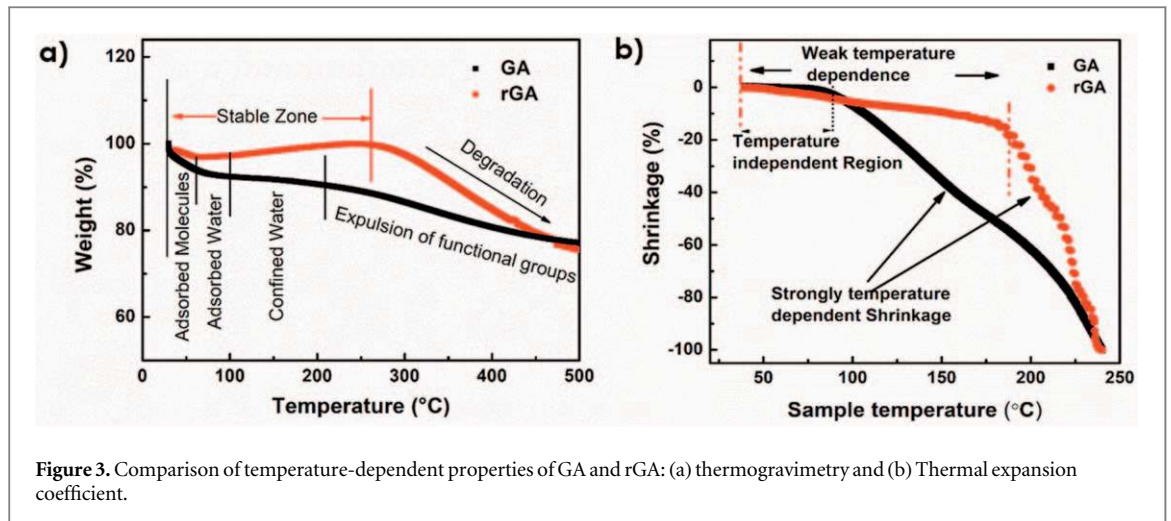
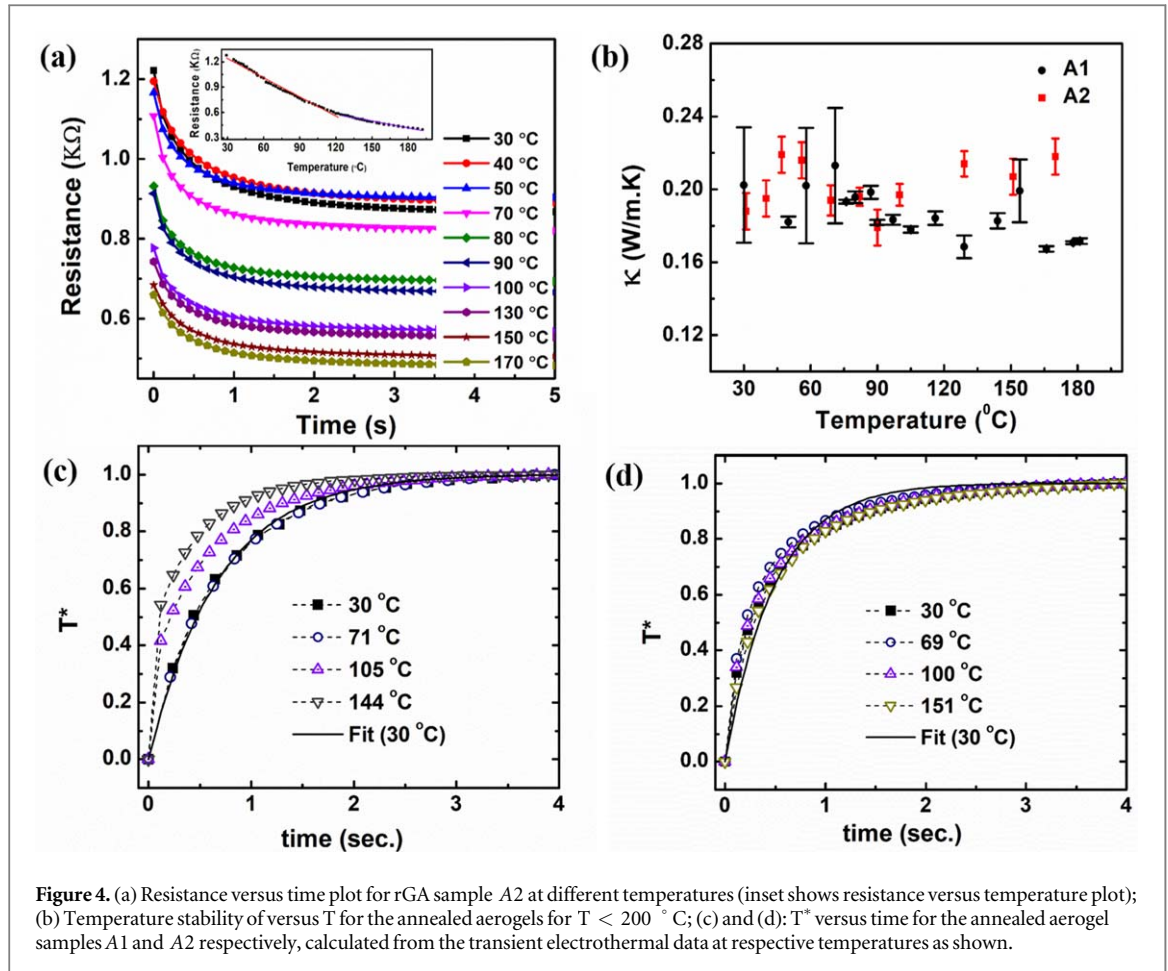


Figure 3. Comparison of temperature-dependent properties of GA and rGA: (a) thermogravimetry and (b) Thermal expansion coefficient.

assigned to the expulsion of the functional groups from GO sheets activated at a temperature higher than the annealing temperature. Nevertheless, the annealed sample shows better thermal stability up to 270 °C without much change in weight. It suggests annealing of the GAs improves the tolerance towards high temperature due to expulsion of functional groups. The trends in the CTE (Model: Dilatometer TA DIL 802) presented in figure 3(b) closely follow the respective in the TGA measurements, with one exception: above 180 °C, rGA sample shows shrinkage even as TGA measurements suggest no loss of weight up to 270 °C. We concur that the primary process responsible for shrinkage of rGA in the interval 180 °C – 250 °C is related to a physical alteration of the porous morphology rather than being associated with large scale loss of functional groups. The annealing restores the sp^2 -hybridization at the flake level and is expected to enhance the electronic conduction at the flake level. The CTE measurements demonstrated profound contraction of the GA samples with increase in temperature. A steady decrease in CTE of $\sim 1.17 \mu\text{m K}^{-1}$ for GA is observed up to the highest temperature (250 °C) in this experiment. We attribute this sample shrinkage to the accompanying loss of oxygen-rich functional groups which results in better $\pi - \pi$ stacking at the flake level and causes shrinkage at the macroscopic level. Furthermore, the process is not reversible i.e. decreasing the temperature does not restore the original dimensions. In comparison, the rGA samples show far superior stability with CTE of $0.21 \mu\text{m K}^{-1}$ up to 180 °C after which the degradation accelerated. Heating the rGA samples to temperatures much higher than the annealing temperature resulted in the same irreversible response.

We next consider thermal transport in rGA samples based on electrothermal techniques. We consider two kinds of samples for thermal studies, by choosing GO/EDA ratio as 0.6×10^3 (sample A1) and 1.1×10^3 (sample A2). The physical model for steady-state electrothermal technique (SET) is based on one-dimensional heat transport which is expressed by a second order differential equation [6]. $q_0 + \kappa \frac{d^2T(x)}{dx^2} = 0$, where ' q_0 ' is heat generated per unit volume due to electrothermal heating, ' T ' is temperature, ' x ' is the position coordinate. For sample with 1D geometry it follows the above equation [6], $\kappa = \frac{q_0 L^2}{12 \Delta T}$, where ' L ' is the sample length and ' ΔT ' is the average temperature rise of the sample over the time of measurement. Here, ΔT is calculated from slope of the $R - T$ plot (Inset of figure 4(a)) and the change in resistance ' ΔR ' due to electrothermal heating as $\Delta T = \Delta R / (R_0 \times p)$, where R_0 is the initial resistance at time $t = 0$ in the SET measurement and as $p = \left(\frac{dR}{dT} \right) / R_i$, where ' R_i ' is the resistance of the sample at room temperature. The SET measurement is carried out by sourcing a step voltage (Keithley 6517B) to a linear strip of sample placed between two copper blocks. Here, it should be noted that the room temperature electrical resistivity of sample A1 and A2 are $0.16 \Omega m$ and $0.28 \Omega m$ respectively. The electro-thermal data at each temperature is shown in figure 4(a) for sample A2 (supplementary file S1 and S2 is available online at stacks.iop.org/MRX/7/105603/mmedia for the corresponding data for sample A1). The corresponding values for κ are obtained from the estimated average temperature rise measured at steady-state, using the above formula and the results are plotted in figure 4(b). The solid thermal conductivities of rGA samples are calculated to be in the same range, $\kappa \sim 0.2 \pm 0.04 \text{ W/mK}$ at room temperature. For this order of thermal conductivity, the radiation contribution can be neglected, and thus our calculation is self-consistent with the original assumption used in the differential equation for heat transport [27]. We briefly compare the magnitude of room temperature thermal conductivity obtained in our sample with literature reports. Low thermal conductivity in a graphene aerogel was reported by Tang *et al* [28] for a system prepared using chemical reduction with paraphenylene diamine in the presence of ammonia. However, their system had comparatively higher density of defects as ascertained from FTIR and TGA studies, and these contributed to the low value of thermal conductivity. Another notable work from Cheng *et al* demonstrated low



thermal conductivity ~ 0.04 W/mK for high-temperature annealed GA and this was attributed to the very fine pore structure achieved in their system with pore size of 3–5 nm [9]. On the other hand, CVD grown mesoporous GA had defect free graphitic structure but the reported thermal conductivity was as high as 182 – 349 W/mK [29]. Thus pore size and defect density are important factors governing the magnitude of thermal conductivity in GA systems. For sample A2, κ is nearly temperature independent throughout the temperature range, while a slight decrease is observed at the higher temperatures up to 180 °C for sample A1. It is possible that when the system undergoes more contraction, then some cracks may propagate which may diminish the thermal conductivity [30]. It is interesting to note that graphene, and hexagonal boron nitride (h-BN) based 3D interconnected networks or aerogels have been embedded in epoxy resin or other polymer matrix to enhance thermal conductivities to values of the order of 2 – 5 W/mK [31]. In all of these cases, the loading fraction of the 2D material is typically high, typically between 1 and 15%. In contrast to these, rarefied and bare rGA networks studied in this work possess an order in magnitude smaller thermal conductivity, and they can be suitable for low-cost thermal insulation which is light-weight and temperature stable.

The transient behaviour of the resistance can be used to estimate the diffusivity of the samples at different temperatures. The average normalised rise in temperature, defined as $T^* = \frac{T(t) - T(0)}{T(t \rightarrow \infty) - T(0)}$ is a good measure of the effectiveness of heat transfer in the sample. T^* of the samples plotted in figures 4(c), (d) has been obtained from the transient region of the electrothermal data using the equation $T^* = \frac{R(t) - R(0)}{R_\infty - R(0)}$ where $R(0)$ and R_∞ are the sample resistances, at time $t = 0$ (before heating) and at steady state (after heating) respectively. The diffusivity can be found out by fitting the above T^* versus t curves (figures 4(c) and (d)) to the solution of the heat transfer equation given by [6]:

$$T^* = \frac{48}{\pi^4} \sum_{m=1}^{\infty} \frac{1 - (-1)^m}{m^2} \left\{ \frac{1 - \exp\left[-\frac{m^2 \pi^2 \alpha_m t}{L^2}\right]}{m^2} \right\},$$

where the quantity α_m is the measured thermal diffusivity and L is the length of the sample. A representative fit to the time-dependent room-temperature data for each sample is shown in figure 4(c) and (d). In summary, weak temperature-dependence for thermal diffusivity was observed for sample A2, with the values fluctuating

between $\sim 1.9 \times 10^{-5} \text{ m}^2 \text{ s}^{-1}$ to $\sim 2.5 \times 10^{-5} \text{ m}^2 \text{ s}^{-1}$ across the temperature interval. For sample A1, weak temperature dependence was observed up to 70°C with value $\sim 1.3 \times 10^{-5} \text{ m}^2 \text{ s}^{-1}$, and thereafter diffusivity increased significantly with temperature, reaching $3.3 \times 10^{-5} \text{ m}^2 \text{ s}^{-1}$ at 144°C . At temperatures above 150°C , the theoretical fits for sample A1 did not faithfully follow the transient data – but the enhancement in diffusivity was nevertheless evident.

How can we understand the physical origin of the trends in the thermal properties, and in particular, the origin of the weak temperature dependence of $\kappa(T)$? Previous studies have looked into thermal transport in unreduced GA networks, but these were limited to cryogenic temperatures on account of the lack of chemical stability at elevated temperatures [6]. On the other hand, heat transport measurements on chemical vapor deposition (CVD) grown graphene foam revealed a strong temperature-dependence for $\kappa(T)$, whose value increased 5-fold for slightly elevated temperatures [32]. However, our system is chemically distinct from both these systems in terms of the nature and density of defects—the former system has a very high defect density while the latter is a mesoporous system chemically closer to being graphitic in nature. We begin by noting that the presence of functionalities in GO significantly alters the thermal transport at the flake level. It is well known that the thermal conductivity of graphite or graphene show characteristic $1/T$ dependence due to Umklapp scattering at high temperatures after achieving a peak value of thermal conductivity below room temperature [33]. In contrast to graphite and graphene, the in-plane thermal conductivity of GO films as well as rGO films remains weakly dependent on temperature in the high temperature interval [34]. The total phonon scattering rate in that bulk (non-aerogel) system is a linear sum of the scattering rates from Umklapp scattering, point defects and sp^2 cluster edges, following Matthiessen's rule with low energy acoustic phonons being the dominant heat carriers. The presence of the remnant oxygen-rich functionalities in reduced graphene-oxide makes the point defect scattering contribution dominant and this contribution has weak temperature dependence. It is not until these bulk GO films are reduced at 1000°C that the point-defect concentration reduces to a small value and Umklapp scattering begins to dominate at elevated temperatures, resulting in $\kappa \sim 1/T$ dependence characteristic of graphite or graphene at such temperatures [33]. In the absence of interfacial effects, the thermal conductivity in aerogels is proportional to the bulk or particle level thermal conductivity and a geometric factor that accounts for the fractal nature of the porous skeleton [34]. The in-plane thermal conductivity of rGO films is in the range of $15 - 20 \text{ W/mK}$ [33], and this value is found to be lower by a factor of 100 in our work due to the formation of an ultralight porous network in rGA. Since the rGA network is composed of rGO flakes reduced at 200°C , and the thermal conductivity at the flake level is weakly temperature-dependent, it follows that the aerogel would also have the same weak temperature-dependence. While the weak temperature-dependent $\kappa(T)$ can be explained by point defect scattering alone, it needs to be examined if interfacial thermal resistance also contributes to the same. Towards this end, we considered the transient electrothermal data, where the measured diffusivity is found to be weakly-dependent on temperature throughout the range (sample A2) or weakly-dependent but increasing after 100°C (sample A1). By considering the microscopic flake-level and interfacial processes, $1/\kappa_{\text{eff}} = 1/\kappa_i + R$ where κ_{eff} is the effective thermal conductivity, κ_i is the intrinsic thermal conductivity at the flake-level and R is the interfacial thermal resistance between overlapping flakes forming the network. Multiplying both sides by $1/\rho C_p$ where ρ is the aerogel density and $C_p(T)$ is the specific heat, we obtain an expression relating effective and intrinsic (flake-level) diffusivities at the microscopic level: $1/\alpha_{\text{eff}} = 1/\alpha_i + R/\rho C_p$. Of the two terms on the right-hand side, the former is an increasing function of temperature since $\alpha_i = \kappa_i/\rho C_p$ where the numerator is weakly-dependent on temperature while the specific heat of all graphitic systems increases with temperature in this interval on account of excitation of additional phonon modes. Since interfacial thermal resistance can also be weakly-dependent on temperature [6], the second term decreases with temperature on account of the specific heat. The microscopic effective diffusivity, α_{eff} , is thus a sum of two factors with opposing temperature-dependences, and this can help to reconcile the weak-temperature dependence inferred for diffusivity for sample A2 and also for sample A1 up to $\sim 100^\circ\text{C}$. To summarize the discussion, when the steady-state and transient electrothermal data are considered together, we infer that both point-defect scattering and interfacial thermal resistance contribute to the weak dependence of thermal conductivity, while any one factor alone is not sufficient to explain the thermal diffusivity trends.

3D porous structures made from interconnected unreduced graphene-oxide are known to possess very low thermal conductivity, although their physical properties change with temperature as functional groups are eliminated. Partial reduction imparts a stable chemical structure at elevated temperatures, even as the remnant functionalities ensure that point-defect phonon scattering at the flake level dominates over Umklapp processes. This, together with interfacial thermal resistance between flakes forming the network contributes to the weak temperature-dependence of the scattering process. Tuning the point-defect density and interfacial bonding can be useful strategies to obtain systems that are both ultra-light as well as temperature-stable thermal insulators. These concepts can also be generalized to other 3D porous structures made from layered two-dimensional materials.

The authors acknowledge financial support from ISRO-IITM cell project no. PHY/1718/177/ISRO/MANJ. We thank AENL, IIT Madras for BET measurements.

Data availability

The data that support the finding of this study are available from the corresponding author upon reasonable request.

ORCID iDs

Manu Jaiswal  <https://orcid.org/0000-0002-8997-4092>

References

- [1] Yao B, Chandrasekaran S, Zhang J, Xiao W, Qian F, Cheng Z, Duoss E B, Spadaccini C M, Worsley M A and Li Y 2019 Efficient 3D printed pseudocapacitive electrodes with ultrahigh MnO₂ loading *Joule* **3** 459–70
- [2] Cavallo C, Agostini M, Genders J P, Abdelhamid M E and Matic A 2019 A free-standing reduced graphene oxide aerogel as supporting electrode in a fluorine-free Li₂S₈ catholyte Li-S battery *J. Power Sources* **416** 111–7
- [3] Hou S, Lv Y, Wu X, Guo J, Sun Q, Wang L and Jia D 2020 Ultralight and highly compressible coal oxide-modified graphene aerogels for organic solvent absorption and light-to-heat conversion *New J. Chem.* **44** 2228–35
- [4] Cheng Y, Tan M, Hu P, Zhang X, Sun B, Yan L, Zhao S and Han W 2018 Strong and thermostable SiC nanowires/graphene aerogel with enhanced hydrophobicity and electromagnetic wave absorption property *Appl. Surf. Sci.* **448** 138
- [5] Xu X *et al* 2019 Double-negative-index ceramic aerogels for thermal superinsulation *Science* **363** 723–7
- [6] Xie Y, Xu S, Xu Z, Wu H, Deng C and Wang X 2016 Interface-mediated extremely low thermal conductivity of graphene aerogel *Carbon* **98** 381–90
- [7] Lu X, Nilsson O, Fricke J and Pekala R W 1993 Thermal and electrical conductivity of monolithic carbon aerogels *J. Appl. Phys.* **73** 581–4
- [8] Pierre A C and Pajonk G M 2002 Chemistry of aerogels and their applications *Chem. Rev.* **102** 4243–65
- [9] Cheng Y, Zhou S, Hu P, Zhao G, Li Y, Zhang X and Han W 2017 Enhanced mechanical, thermal, and electric properties of graphene aerogels via supercritical ethanol drying and high-temperature thermal reduction *Sci. Rep.* **7** 1439
- [10] Zhu X *et al* 2020 Precise control of versatile microstructure and properties of graphene aerogel via freezing manipulation *Nanoscale* **12** 4882–94
- [11] Wang J, Huang J, Yan R, Wang F, Cheng W, Guo Q and Wang J 2015 Graphene microsheets from natural microcrystalline graphite minerals: scalable synthesis and unusual energy storage *J. Mater. Chem. A* **3** 3144–50
- [12] Loh K P, Bao Q, Eda G and Chhowalla M 2010 Graphene oxide as a chemically tunable platform for optical applications *Nat. Chem.* **2** 1015–24
- [13] Acik M, Lee G, Mattevi C, Pirkle A, Wallace R M, Chhowalla M, Cho K and Chabal Y 2011 The role of oxygen during thermal reduction of graphene oxide studied by infrared absorption spectroscopy *J. Phys. Chem. C* **115** 19761–81
- [14] Dave S H, Gong C, Robertson A W, Warner J H and Grossman J C 2016 Chemistry and structure of graphene oxide via direct imaging *ACS Nano* **10** 7515–22
- [15] Ghosh M, Pradipkanti L, Rai V, Satapathy D K, Vayalankuzhi P and Jaiswal M 2015 Confined water layers in graphene oxide probed with spectroscopic ellipsometry *Appl. Phys. Lett.* **106** 241902
- [16] Sakorikar T, Kavitha M K, Vayalankuzhi P and Jaiswal M 2017 Thickness-dependent crack propagation in uniaxially strained conducting graphene oxide films on flexible substrates *Sci. Rep.* **7** 2598 (1–10)
- [17] Eda G, Mattevi C, Yamaguchi H, Kim H and Chhowalla M 2009 Insulator to semimetal transition in graphene oxide *J. Phys. Chem. C* **113** 15768–71
- [18] Crane M J, Lim M B, Zhou X and Pauzaskie P J 2017 Rapid synthesis of transition metal dichalcogenide–carbon aerogel composites for supercapacitor electrodes *Microsystems & Nanoengineering* **3** 17032
- [19] Liang J, Cai Z, Li L, Guo L and Geng J 2014 Scalable and facile preparation of graphene aerogel for air purification *RSC Adv.* **4** 4843–7
- [20] Gao C, Dong Z, Hao X, Yao Y and Guo S 2020 Preparation of reduced graphene oxide aerogel and its adsorption for Pb(II) *ACS Omega* **5** 9903–11
- [21] Liao Y, Huang Y, Shu D, Zhong Y, Hao J, He C, Zhong J and Song X 2016 Three-dimensional nitrogen-doped graphene hydrogels prepared via hydrothermal synthesis as high-performance supercapacitor materials *Electrochim. Acta* **194** 136–42
- [22] Luo Z J, Geng H Z, Zhang X, Du B, Ding E X, Wang J, Lu Z, Sun B, Wang J and Liu J 2016 A timesaving, low-cost, high-yield method for the synthesis of ultrasmall uniform graphene oxide nanosheets and their application in surfactants *Nanotechnology* **27** 055601
- [23] Gong Y, Li D, Fu Q and Pan C 2015 Influence of graphene microstructures on electrochemical performance for supercapacitors *Progress in Natural Science: Materials International* **25** 379–85
- [24] Szabó T, Berkesi O and Dékány I 2005 DRIFT study of deuterium-exchanged graphite oxide *Carbon* **43** 3186–9
- [25] Tuinstra F and Koenig J L 1970 Raman spectrum of graphite *J. Chem. Phys.* **53** 1126–30
- [26] Wang Z L, Xu D, Huang Y, Wu Z, Wang L and Zhang X 2012 Facile, mild and fast thermal-decomposition reduction of graphene oxide in air and its application in high performance lithium batteries *Chem. Commun.* **48** 976–8
- [27] Lu X, Arduini-Schuster M C, Kuhn J, Nilsson O, Fricke J and Pekala R W 1992 Thermal conductivity of monolithic organic aerogels *Science* **255** 971–2
- [28] Tang G, Jiang Z G, Li X, Zhang H B, Dasari A and Yu Z Z 2014 Three dimensional graphene aerogels and their electrically conductive composites *Carbon* **77** 592–9
- [29] Lin H, Xu S, Wang X and Mei N 2013 Significantly reduced thermal diffusivity of free-standing two-layer graphene in graphene foam *Nanotechnology* **24** 415706
- [30] Xu X, Zhang Q, Yu Y, Chen W, Hu H and Li H 2016 Naturally dried graphene aerogels with super elasticity and tunable Poisson's Ratio *Adv. Mater.* **28** 9223–30

- [31] Song H, Liu J, Liu B, Wu J, Cheng H M and Kang F 2018 Two-dimensional materials for thermal management applications *Joule* **2** 442–63
- [32] Li M, Sun Y, Xiao H, Hu X and Yue Y 2015 High temperature dependence of thermal transport in graphene foam *Nanotechnology* **26** 105703
- [33] Renteria J D, Ramirez S, Malekpour H, Alonso B, Centeno A, Zurutuza A, Cocemasov A I, Nika D L and Balandin A A 2015 Strongly anisotropic thermal conductivity of free-standing reduced graphene oxide films annealed at high temperature *Adv. Funct. Mater.* **25** 4664–72
- [34] Emmerling A and Fricke J 1997 Scaling properties and structure of aerogels *J. Sol-Gel Sci. Technol.* **8** 781–8